

A superconvergent point interpolation method (SC-PIM) with piecewise linear strain field using triangular mesh

G. R. Liu^{1,3}, X. Xu^{2,3,4,*},†, G. Y. Zhang³ and T. Nguyen-Thoi¹

¹*Centre for Advanced Computations in Engineering Science (ACES), Department of Mechanical Engineering, National University of Singapore, 9 Engineering Drive 1, 117576 Singapore, Singapore*

²*Department of Mechanics at School of Science, Beijing Institute of Technology, No. 5, Zhongguancun Nandajie, Beijing 100081, People's Republic of China*

³*Singapore-MIT Alliance (SMA), E4-04-10, 4 Engineering Drive 3, 117576 Singapore, Singapore*

⁴*College of Mathematics, Jilin University, 2699 Qianjin Street, Changchun 130012, People's Republic of China*

SUMMARY

A superconvergent point interpolation method (SC-PIM) is developed for mechanics problems by combining techniques of finite element method (FEM) and linearly conforming point interpolation method (LC-PIM) using triangular mesh. In the SC-PIM, point interpolation methods (PIM) are used for shape functions construction; and a strain field with a parameter α is assumed to be a linear combination of compatible strains and smoothed strains from LC-PIM. We prove theoretically that SC-PIM has a very nice bound property: the strain energy obtained from the SC-PIM solution lies in between those from the compatible FEM solution and the LC-PIM solution when the same mesh is used. We further provide a criterion for SC-PIM to obtain upper and lower bound solutions. Intensive numerical studies are conducted to verify these theoretical results and show that (1) the upper and lower bound solutions can always be obtained using the present SC-PIM; (2) there exists an $\alpha_{\text{exact}} \in (0, 1)$ at which the SC-PIM can produce the exact solution in the energy norm; (3) for any $\alpha \in (0, 1)$ the SC-PIM solution is of superconvergence, and $\alpha = 0$ is an easy way to obtain a very accurate and superconvergent solution in both energy and displacement norms; (4) a procedure is devised to find a $\alpha_{\text{prefer}} \in (0, 1)$ that produces a solution very close to the exact solution. Copyright © 2008 John Wiley & Sons, Ltd.

Received 6 December 2007; Revised 16 July 2008; Accepted 4 August 2008

KEY WORDS: meshfree methods; finite element method; point interpolation method; solution bound; superconvergence; Hellinger–Reissner's variational principle

*Correspondence to: X. Xu, Department of Mechanics at School of Science, Beijing Institute of Technology, No. 5, Zhongguancun Nandajie, Beijing 100081, People's Republic of China.

†E-mail: Xuxu@jlu.edu.cn, Smaxx@nus.edu.sg

Contract/grant sponsor: National Natural Science Foundation of China; contract/grant numbers: 10532050, 10501017, 60673023

Contract/grant sponsor: 985 Program of Jilin University, China

Contract/grant sponsor: Centre for ACES and Singapore-MIT Alliance (SMA), National University of Singapore

1. INTRODUCTION

The development of meshfree methods has achieved remarkable progress in recent years. Methods and techniques developed so far include the smooth particle hydrodynamic (SPH) method [1–4], the diffuse element method (DEM) [5], the element-free Galerkin (EFG) method [6], the reproducing kernel particle method (RKPM) [7], the meshless local Petrov–Galerkin (MLPG) method [8], the point interpolation method (PIM) [9, 10], Kriging interpolation method [11–13], etc. A very detailed introduction on many types of meshfree methods and techniques for different problems can be found in books [2, 14] and the source codes of some methods can also be found in [2, 15]. These methods and techniques extend our minds in the quest for more effective and robust computational methods.

The linearly conforming point interpolation method (LC-PIM) [16, 17] is evolved from the point interpolation method (PIM) with the use of gradient smoothing technique [18]. It is formulated based on the generalized Galerkin weak form and the PIM shape functions constructed employing point interpolation procedure using a small set of nodes located in a local support domain that can be overlapping [9, 10]. A more general form called LC-RPIM [19, 20] is also developed based on the radial PIM that uses radial basis functions and hence works well for extremely irregular node distributions [10, 14]. A good feature of PIM and RPIM shape functions is that they possess Delta function property, which allows straightforward imposition of essential boundary conditions. A very important property of LC-PIM and LC-RPIM is that they provide an upper bound solution in energy norm for elasticity problems with homogenous essential boundary conditions [21, 22]. This implies that the LC-PIM can produce a ‘softer’ stiffness matrix than the actual solid under analysis.

The finite element method (FEM) has been used most widely for engineering problems. It is well known that the displacement-based fully compatible FEM provides a lower bound in energy norm for the exact solution to elasticity problems [23–25]. This fact implies that an FEM model result in a ‘stiffer’ stiffness matrix. Thus, using both LC-PIM (LC-RPIM) and FEM, we can obtain certified solutions with both upper and lower bounds [26].

The important point is that FEM and LC-PIM play complementary roles in the numerical analysis for solution bounds. Thus, a question naturally arises: can we develop a method to improve the accuracy of the numerical solution by combining the good features of two methods into a single numerical method? If this can be done, it can provide a new means to obtain superconvergent and even nearly exact solutions.

In this paper, a superconvergent point interpolation method (SC-PIM) is proposed using the existing FEM and LC-PIM techniques. A parameter is equipped in the SC-PIM for superconvergent solutions. By adjusting the parameter, not only the upper bound but also the lower bound of the exact solution in energy norm is obtained using the same mesh. Furthermore, a solution that is as close as possible to the exact solution can be obtained using a finite number of triangular elements.

This paper is outlined as follows. Sections 2 and 3 brief on the linear elasticity and LC-PIM. The idea of the SC-PIM is presented in Section 4. The properties of the SC-PIM are presented and corresponding theoretically proven in Sections 5 and 6. In Section 7, the unique superconvergence of the SC-PIM is discussed. In Section 8, numerical examples are presented and discussed to verify the formulations and properties of the SC-PIM. Conclusions and remarks are made in Section 9.

2. BASIC EQUATIONS FOR LINEARITY ELASTICITY PROBLEMS

Consider a 2D static elasticity problem governed by the equilibrium equation in the domain Ω bounded by Γ ($\Gamma = \Gamma_u + \Gamma_t$, $\Gamma_u \cap \Gamma_t = 0$) as

$$\mathbf{L}_d^T \boldsymbol{\sigma} + \mathbf{b} = 0 \quad \text{in } \Omega \quad (1)$$

where \mathbf{L}_d is a matrix of differential operators defined as

$$\mathbf{L}_d = \begin{bmatrix} \frac{\partial}{\partial x} & 0 & \frac{\partial}{\partial y} \\ 0 & \frac{\partial}{\partial y} & \frac{\partial}{\partial x} \end{bmatrix}^T \quad (2)$$

$\boldsymbol{\sigma}^T = (\sigma_{xx}, \sigma_{yy}, \sigma_{xy})$ is the vector of stresses, $\mathbf{b}^T = (b_x, b_y)$ is the vector of body forces. The stresses relate the strains via the generalized Hook's law:

$$\boldsymbol{\sigma} = \mathbf{D} \boldsymbol{\varepsilon} \quad (3)$$

where \mathbf{D} is the matrix of material constants, and $\boldsymbol{\varepsilon}^T = (\varepsilon_{xx}, \varepsilon_{yy}, \gamma_{xy})$ is the vector of strains given by

$$\boldsymbol{\varepsilon} = \mathbf{L}_d \mathbf{u} \quad (4)$$

Essential boundary conditions are

$$\mathbf{u} = \mathbf{u}_0 \quad \text{on } \Gamma_u \quad (5)$$

where $\mathbf{u}^T = (u_x, u_y)$ is the vector of the displacement and \mathbf{u}_0 is the vector of the prescribed displacements on the essential boundary Γ_u . In this paper, we consider only homogenous essential boundary conditions $\mathbf{u}_0 = \mathbf{0}$.

Natural boundary conditions are

$$\mathbf{L}_n^T \boldsymbol{\sigma} = \mathbf{T} \quad \text{on } \Gamma_t \quad (6)$$

where \mathbf{T} is the vector of the prescribed tractions on the natural boundary Γ_t , and \mathbf{L}_n is the matrix of unit outward normal, which can be expressed as

$$\mathbf{L}_n = \begin{bmatrix} n_x & 0 & n_y \\ 0 & n_y & n_x \end{bmatrix}^T \quad (7)$$

3. BRIEFING ON THE LC-PIM [16, 17]

In the LC-PIM, the displacements are approximated as follows:

$$\bar{\mathbf{u}}(x) = \sum_{i \in n_e} \Phi_i(\mathbf{x}) \bar{\mathbf{d}}_i \quad (8)$$

where n_e is the set of nodes of the local support domain containing \mathbf{x} , $\bar{\mathbf{d}}_i$ is a vector of displacements at this set of nodes, and

$$\Phi_i(\mathbf{x}) = \begin{bmatrix} \varphi_i(\mathbf{x}) & 0 \\ 0 & \varphi_i(\mathbf{x}) \end{bmatrix} \tag{9}$$

is the shape functions matrix for node i , which are generally constructed using the PIM procedure.

In carrying out the numerical integration, the problem domain Ω is divided into smoothing domains Ω_k containing node k , as shown in Figure 1. LC-PIM uses constant strain for each of the smoothing domain defined by [18]

$$\bar{\boldsymbol{\varepsilon}}_k \equiv \bar{\boldsymbol{\varepsilon}}(\mathbf{x}_k) = \frac{1}{A_k} \int_{\Omega_k} \tilde{\boldsymbol{\varepsilon}}(\mathbf{x}) \, d\Omega \tag{10}$$

where $A_k = \int_{\Omega_k} d\Omega$ is the area of smoothing domain for node k , and $\tilde{\boldsymbol{\varepsilon}}(\mathbf{x}) = \mathbf{L}_d \bar{\mathbf{u}}$ is the compatible strain.

Because the LC-PIM is variationally consistent as proven (when the solutions is sought in an H space) in [21], the assumed displacement $\bar{\mathbf{u}}$ and the corresponding assumed strains $\bar{\boldsymbol{\varepsilon}}$ satisfy the generalized Galerkin weak form

$$\int_{\Omega} \delta \bar{\boldsymbol{\varepsilon}}^T(\bar{\mathbf{u}}) \mathbf{D} \bar{\boldsymbol{\varepsilon}}(\bar{\mathbf{u}}) \, d\Omega - \int_{\Omega} \delta \bar{\mathbf{u}}^T \mathbf{b} \, d\Omega - \int_{\Gamma_t} \delta \bar{\mathbf{u}}^T \mathbf{T} \, d\Gamma = 0 \tag{11}$$

Substituting Equations (8) and (10) into Equation (11) yields the discretized system equation:

$$\bar{\mathbf{K}} \bar{\mathbf{d}} = \bar{\mathbf{f}} \tag{12}$$

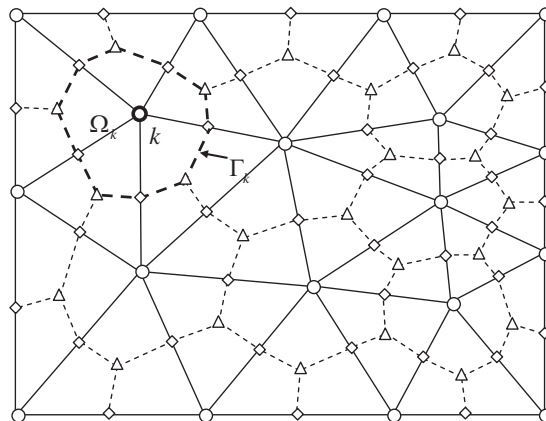


Figure 1. Triangular elements and the smoothing cells in the LC-PIM. o, Field node; ◇, mid-edge-point; and △, centroid of triangle.

where

$$\bar{\mathbf{K}} = \sum_{k=1}^N \bar{\mathbf{K}}_{ij}^{(k)} = \sum_{k=1}^N \int_{\Omega_k} \bar{\mathbf{B}}_i^T(\mathbf{x}_k) \mathbf{D} \bar{\mathbf{B}}_j^T(\mathbf{x}_k) d\Omega \quad (13)$$

$$\bar{\mathbf{f}}_i = \int_{\Gamma_i} \varphi_i \mathbf{T} d\Gamma + \int_{\Omega} \varphi_i \mathbf{b} d\Omega \quad (14)$$

$$\bar{\mathbf{B}}_i(\mathbf{x}_k) = \begin{bmatrix} \bar{b}_{ix}(\mathbf{x}_k) & 0 \\ 0 & \bar{b}_{iy}(\mathbf{x}_k) \\ \bar{b}_{iy}(\mathbf{x}_k) & \bar{b}_{ix}(\mathbf{x}_k) \end{bmatrix} \quad (15)$$

$$\bar{b}_{il}(\mathbf{x}_k) = \frac{1}{A_k} \sum_{m=1}^{N_s} \left[\sum_{n=1}^{N_g} w_n \varphi_i(\mathbf{x}_{mn}) n_l(\mathbf{x}_m) \right], \quad (l=x, y) \quad (16)$$

4. THE IDEA OF THE SC-PIM

4.1. Choice of the shape functions

Note that background cells have to be used for performing the numerical integration in meshfree methods and the triangular cells that can be generalized automatically are the most convenient [14]. Therefore, the present SC-PIM uses the background cells of 3-node triangles for shape functions construction as well as for strain field construction as in the LC-PIM, which ensures efficiency and reliability. Once the PIM shape functions are created, the displacements can be approximated as follows:

$$\hat{\mathbf{u}}(\mathbf{x}) = \sum_{i \in n_e} \Phi_i(\mathbf{x}) \hat{\mathbf{d}}_i \quad (17)$$

where n_e is the set of nodes in the support domain containing \mathbf{x} , $\hat{\mathbf{d}}_i$ is the vector of nodal displacements and $\Phi_i(\mathbf{x})$ is the matrix of the PIM shape functions for node i as shown in Equation (9).

4.2. Assumption for strain field

In the present SC-PIM, the problem domain Ω is divided into a set of smoothing domains Ω_k containing node k as shown in Figure 1. By connecting node k to the centroids of the surrounding triangles, the Ω_k is further sub-divided into M sub-domains $\Omega_{k,1}, \Omega_{k,2}, \dots, \Omega_{k,M}$ and the union of all $\Omega_{k,i}$ forms Ω_k exactly, as shown in Figure 2.

We now assume that the strain $\hat{\boldsymbol{\varepsilon}}$ at any points within any sub-domain $\Omega_{k,i}$ for $k=1, 2, \dots, N$, $i=1, 2, \dots, M$ varies linearly:

$$\hat{\boldsymbol{\varepsilon}} = L_1 \boldsymbol{\varepsilon}_k + L_2 \boldsymbol{\varepsilon}_P + L_3 \boldsymbol{\varepsilon}_I \quad (18)$$

where L_1, L_2, L_3 are the area coordinates for sub-triangular $\Omega_{k,i}$; $\boldsymbol{\varepsilon}_k, \boldsymbol{\varepsilon}_P, \boldsymbol{\varepsilon}_I$ are the assumed strains at the node k , mid-edge-points P and the centroid I of the surrounding triangles of nodes k , respectively.

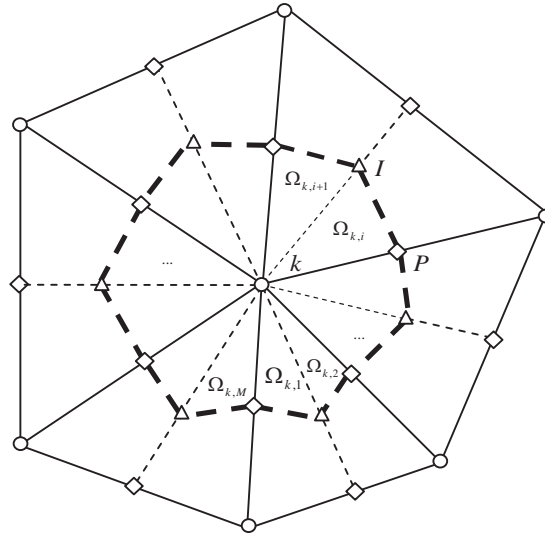


Figure 2. Illustration of background triangular sub-domains $\Omega_{k,i}$ used for linear strain field construction. \circ , Field node; \diamond , mid-edge-point; and \triangle , centroid of triangle.

The strains $\boldsymbol{\varepsilon}_k, \boldsymbol{\varepsilon}_P, \boldsymbol{\varepsilon}_I$ can be assumed in a number of schemes.

Scheme 1. We assume $\boldsymbol{\varepsilon}_k = \mathbf{L}_d \hat{\mathbf{u}}(\mathbf{x}_k), \boldsymbol{\varepsilon}_P = \mathbf{L}_d \hat{\mathbf{u}}(\mathbf{x}_P), \boldsymbol{\varepsilon}_I = \mathbf{L}_d \hat{\mathbf{u}}(\mathbf{x}_I)$.

In this case, the SC-PIM will be exactly the same as the FEM when the linear polynomial interpolation is used.

Scheme 2. We assume $\boldsymbol{\varepsilon}_k = \boldsymbol{\varepsilon}_P = \boldsymbol{\varepsilon}_I = \bar{\boldsymbol{\varepsilon}}_k \equiv (1/A_k) \int_{\Omega_k} \mathbf{L}_d \hat{\mathbf{u}} d\Omega$.

In this case, the SC-PIM becomes the LC-PIM [16, 21].

Scheme 3. We assume

$$\boldsymbol{\varepsilon}_k = \boldsymbol{\varepsilon}_P = \bar{\boldsymbol{\varepsilon}}_k \equiv \frac{1}{A_k} \int_{\Omega_k} \mathbf{L}_d \hat{\mathbf{u}} d\Omega \tag{19}$$

$$\boldsymbol{\varepsilon}_I = \alpha \bar{\boldsymbol{\varepsilon}}_k + (1 - \alpha) \tilde{\boldsymbol{\varepsilon}}_{k,i}, \quad (0 \leq \alpha \leq 1) \tag{20}$$

where $\tilde{\boldsymbol{\varepsilon}}_{k,i} = \mathbf{L}_d \hat{\mathbf{u}}_{k,i}$ is the compatible stain, and $\hat{\mathbf{u}}_{k,i}$ obtained using Equation (17) is the assumed displacement in sub-domain $\Omega_{k,i}$. In this case, the SC-PIM produces a linear strain field that is piecewise linear and C^0 continuous in the smoothing cell Ω_k .

4.3. Variational formulation for SC-PIM

According to Hellinger–Reissner’s two-field variational principle [27–29], we construct the following energy functional for the discretized system equations:

$$\Pi(\mathbf{v}) = \int_{\Omega} -\frac{1}{2} \hat{\boldsymbol{\varepsilon}}^T(\mathbf{v}) \mathbf{D} \hat{\boldsymbol{\varepsilon}}(\mathbf{v}) d\Omega + \int_{\Omega} \hat{\boldsymbol{\varepsilon}}^T(\mathbf{v}) \mathbf{D}(\mathbf{L}_d \mathbf{v}) d\Omega - \int_{\Omega} \mathbf{v}^T \mathbf{b} d\Omega - \int_{\Gamma_t} \mathbf{v}^T \mathbf{T} d\Gamma \tag{21}$$

Substituting Equations (18)–(21), the stationary condition leads to the following discretized system equations with the matrix form:

$$\hat{\mathbf{K}} \hat{\mathbf{d}} = \hat{\mathbf{f}} \tag{22}$$

where

$$\hat{\mathbf{f}} = - \int_{\Omega} \Phi^T \mathbf{b} d\Omega + \int_{\Gamma_t} \Phi^T \mathbf{T} d\Gamma \quad (23)$$

and $\hat{\mathbf{K}}$ is the stiffness matrix and will be given in detail later.

The overall procedure of strain field construction in the SC-PIM is as follows. The displacement at any point in a cell is first approximated via point interpolation using Equation (17). The strains at points k, P and I are then evaluated using Equations (19) and (20). The strain field is next constructed again via point interpolation using Equation (18).

Note that the construction of strain field $\hat{\boldsymbol{\varepsilon}}$ in SC-PIM is based on the displacement field \mathbf{v} . Hence, the displacement field is the only unknown field and there is no increase of extra unknown variables compared with the standard Galerkin formulation.

Owing to the smoothing operation, the assumed strain in LC-PIM is constant in each smoothing domain Ω_k . LC-PIM hence gives the simple averaged behavior in the smoothing domain Ω_k ; while strain difference in the individual triangular sub-domains $\Omega_{k,i}$ is ignored. In the FEM, on the other hand, the strain in each individual sub-domain gives the full consideration of the local behavior of $\Omega_{k,i}$ and does not consider the overall behavior of Ω_k . The SC-PIM considers not only the averaged behavior of Ω_k but also the local effects of $\Omega_{k,i}$ and it hence has many excellent features that will be examined in the following sections.

5. BOUND PROPERTIES OF THE SC-PIM STRAIN ENERGY POTENTIAL

In the PIMs, there are many ways to choose the interpolation points for shape functions construction. For simplification and in comparison with the bound properties of the FEM solutions, we only consider the linear polynomials interpolation. In this case, the displacement is continuous and hence is in an H space,[‡] the compatible strain $\mathbf{L}_d \mathbf{v}$ is constant in each of the triangular cells for a given linear displacement \mathbf{v} .

Theorem 1

For any given admissible linear displacement field \mathbf{v} , the strains at any points within sub-domain $\Omega_{k,i}$ are obtained using Equations (18)–(20), and Equation (21) is used to produce discretized system equations. We then have

$$\bar{U}(\mathbf{v}) \leq \hat{U}(\mathbf{v}) \leq \tilde{U}(\mathbf{v}) \quad (24)$$

where $\hat{U}(\mathbf{v})$ is the strain energy obtained from the SC-PIM solution given by

$$\hat{U}(\mathbf{v}) = \sum_{k=1}^N \sum_{i=1}^M \left[-\frac{1}{2} \int_{\Omega_{k,i}} \hat{\boldsymbol{\varepsilon}}_{k,i}^T(\mathbf{v}) \mathbf{D} \hat{\boldsymbol{\varepsilon}}_{k,i}(\mathbf{v}) d\Omega + \int_{\Omega_{k,i}} \hat{\boldsymbol{\varepsilon}}_{k,i}^T(\mathbf{v}) \mathbf{D} \tilde{\boldsymbol{\varepsilon}}_{k,i}(\mathbf{v}) d\Omega \right] \quad (25)$$

[‡]When a discontinuous displacement functions are used, it would be in a G space. The proof on this is more involved and will be presented in our future work. In this work, the admissible field refers a field living in an H space.

$\tilde{U}(\mathbf{v})$ is that of the FEM model given by

$$\tilde{U}(\mathbf{v}) = \sum_{k=1}^N \sum_{i=1}^M \frac{1}{2} \int_{\Omega_{k,i}} \tilde{\boldsymbol{\varepsilon}}_{k,i}^T(\mathbf{v}) \mathbf{D} \tilde{\boldsymbol{\varepsilon}}_{k,i}(\mathbf{v}) \, d\Omega \tag{26}$$

and $\bar{U}(\mathbf{v})$ is that of the LC-PIM model given by

$$\bar{U}(\mathbf{v}) = \sum_{k=1}^N \frac{1}{2} \int_{\Omega_k} \bar{\boldsymbol{\varepsilon}}_k^T(\mathbf{v}) \mathbf{D} \bar{\boldsymbol{\varepsilon}}_k(\mathbf{v}) \, d\Omega \tag{27}$$

Proof

The strain energy potential of SC-PIM in Equation (21) can be written as

$$\begin{aligned} \hat{U}(\mathbf{v}) &= \sum_{k=1}^N \sum_{i=1}^M \left[-\frac{1}{2} \int_{\Omega_{k,i}} \hat{\boldsymbol{\varepsilon}}_{k,i}^T(\mathbf{v}) \mathbf{D} \hat{\boldsymbol{\varepsilon}}_{k,i}(\mathbf{v}) \, d\Omega + \int_{\Omega_{k,i}} \hat{\boldsymbol{\varepsilon}}_{k,i}^T(\mathbf{v}) \mathbf{D} \tilde{\boldsymbol{\varepsilon}}_{k,i}(\mathbf{v}) \, d\Omega \right] \\ &= \sum_{k=1}^N \sum_{i=1}^M \hat{U}_{k,i}(\mathbf{v}) \end{aligned} \tag{28}$$

where

$$\hat{U}_{k,i}(\mathbf{v}) = -\frac{1}{2} \int_{\Omega_{k,i}} \hat{\boldsymbol{\varepsilon}}_{k,i}^T \mathbf{D} \hat{\boldsymbol{\varepsilon}}_{k,i} \, d\Omega + \int_{\Omega_{k,i}} \hat{\boldsymbol{\varepsilon}}_{k,i}^T \mathbf{D} \tilde{\boldsymbol{\varepsilon}}_{k,i} \, d\Omega \tag{29}$$

Substituting (18) into (29) and using the following formula [25],

$$\int_A L_1^p L_2^q L_3^r \, dA = \frac{p!q!r!}{(p+q+r+2)!} 2A \tag{30}$$

we have

$$\begin{aligned} \hat{U}_{k,i}(\mathbf{v}) &= -\frac{1}{12} (3 + 2\alpha + \alpha^2) A_{k,i} (\bar{\boldsymbol{\varepsilon}}_k - \tilde{\boldsymbol{\varepsilon}}_{k,i})^T \mathbf{D} (\bar{\boldsymbol{\varepsilon}}_k - \tilde{\boldsymbol{\varepsilon}}_{k,i}) + \frac{1}{2} A_{k,i} \hat{\boldsymbol{\varepsilon}}_{k,i}^T \mathbf{D} \tilde{\boldsymbol{\varepsilon}}_{k,i} \\ &\leq \frac{1}{2} \int_{\Omega_{k,i}} \tilde{\boldsymbol{\varepsilon}}_{k,i}^T(\mathbf{v}) \mathbf{D} \tilde{\boldsymbol{\varepsilon}}_{k,i}(\mathbf{v}) \, d\Omega = \tilde{U}_{k,i}(\mathbf{v}) \end{aligned} \tag{31}$$

and

$$\sum_{i=1}^M \hat{U}_{k,i}(\mathbf{v}) = \frac{1}{12} (3 - 2\alpha - \alpha^2) \left[\sum_{i=1}^M A_{k,i} \hat{\boldsymbol{\varepsilon}}_{k,i}^T \mathbf{D} \tilde{\boldsymbol{\varepsilon}}_{k,i} - A_k \bar{\boldsymbol{\varepsilon}}_k^T \mathbf{D} \bar{\boldsymbol{\varepsilon}}_k \right] + \frac{1}{2} A_k \bar{\boldsymbol{\varepsilon}}_k^T \mathbf{D} \bar{\boldsymbol{\varepsilon}}_k \tag{32}$$

By the positivity of elasticity constant matrix \mathbf{D} , we have

$$\begin{aligned} &\sum_{i=1}^M [\sqrt{A_{k,i}} \bar{\boldsymbol{\varepsilon}}_k - \sqrt{A_{k,i}} \tilde{\boldsymbol{\varepsilon}}_{k,i}]^T \mathbf{D} [\sqrt{A_{k,i}} \bar{\boldsymbol{\varepsilon}}_k - \sqrt{A_{k,i}} \tilde{\boldsymbol{\varepsilon}}_{k,i}] \\ &= \sum_{i=1}^M [A_{k,i} \bar{\boldsymbol{\varepsilon}}_k^T \mathbf{D} \bar{\boldsymbol{\varepsilon}}_k - 2A_{k,i} \bar{\boldsymbol{\varepsilon}}_k^T \mathbf{D} \tilde{\boldsymbol{\varepsilon}}_{k,i} + A_{k,i} \tilde{\boldsymbol{\varepsilon}}_{k,i}^T \mathbf{D} \tilde{\boldsymbol{\varepsilon}}_{k,i}] = -A_k \bar{\boldsymbol{\varepsilon}}_k^T \mathbf{D} \bar{\boldsymbol{\varepsilon}}_k + \sum_{i=1}^M A_{k,i} \tilde{\boldsymbol{\varepsilon}}_{k,i}^T \mathbf{D} \tilde{\boldsymbol{\varepsilon}}_{k,i} \geq 0 \end{aligned} \tag{33}$$

or

$$\sum_{i=1}^M A_{k,i} \tilde{\mathbf{e}}_{k,i}^T \mathbf{D} \tilde{\mathbf{e}}_{k,i} \geq A_k \bar{\mathbf{e}}_k^T \mathbf{D} \bar{\mathbf{e}}_k \quad (34)$$

Substituting Equation (34) into (32) gives

$$\sum_{i=1}^N \hat{U}_{k,i}(\mathbf{v}) \geq \frac{1}{2} A_k \bar{\mathbf{e}}_k^T \mathbf{D} \bar{\mathbf{e}}_k = \frac{1}{2} \int_{\Omega_k} \bar{\mathbf{e}}_k^T(\mathbf{v}) \mathbf{D} \bar{\mathbf{e}}_k(\mathbf{v}) \, d\Omega \quad (35)$$

In deriving above equation, we have used the fact $3 - 2\alpha - \alpha^2 \geq 0$ when $0 \leq \alpha \leq 1$.

Equations (31) and (35) give

$$\bar{U}(\mathbf{v}) \leq \sum_{k=1}^N \sum_{i=1}^M \hat{U}_{k,i}(\mathbf{v}) \leq \tilde{U}(\mathbf{v}) \quad (36)$$

which completes the proof. \square

Remark

It is clear from the proof of Theorem 1 that when the PIM Shape functions with polynomial bases are used, exact integration is readily available, and no numerical integration is needed.

Corollary 1

The stiffness matrix $\hat{\mathbf{K}}$ obtained from SC-PIM is symmetry and has the same dimension as the FEM and LC-PIM, when the same mesh and node numbering are used.

Corollary 1 is obvious from Equation (32).

Theorem 2

When the same mesh is used, the strain energy obtained from the SC-PIM solution is no-less than that from the FEM solution based on a fully compatible model, and no-larger than the strain potential for the LC-PIM model:

$$\frac{1}{2} \tilde{\mathbf{d}}^T \tilde{\mathbf{K}} \tilde{\mathbf{d}} \leq \frac{1}{2} \hat{\mathbf{d}}^T \hat{\mathbf{K}} \hat{\mathbf{d}} \leq \frac{1}{2} \bar{\mathbf{d}}^T \bar{\mathbf{K}} \bar{\mathbf{d}} \quad (37)$$

The proof of Theorem 2 is similar to that given in Reference [21] and thus is omitted.

6. LOWER AND UPPER BOUNDS OF THE SC-PIM SOLUTION

The fully compatible FEM can usually produce the lower bound solution in energy norm for the exact solution to the elasticity problems [23–25]. However, this property of FEM may or may not stand for SC-PIM. In the SC-PIM, the strain energy is calculated using the simple linear combinations of the compatible and the smoothed strains that are all obtained using the assumed displacement, and hence the displacement field is the only unknown variable. Therefore, the strain energy from Equation (32) is still a quadratic function of the displacement function for a given α . However, the value of α can influence the bound property of SC-PIM.

Here we consider a situation when SC-PIM model is sufficiently fine so that the solution is *reasonably* close to the exact solution. We can then determine the bound properties of the present

SC-PIM, by assuming the displacement field of SC-PIM in the form of $\mathbf{v}=\mathbf{u}+\delta\mathbf{v}$ where \mathbf{u} is the exact solution and $\delta\mathbf{v}$ is an arbitrarily small error. The corresponding assumed strain field and stress field can now expressed, respectively, as $\hat{\boldsymbol{\sigma}}=\boldsymbol{\sigma}+\delta\hat{\boldsymbol{\sigma}}$ and $\hat{\boldsymbol{\varepsilon}}=\boldsymbol{\varepsilon}+\delta\hat{\boldsymbol{\varepsilon}}$, which are the functions only of displacement field \mathbf{v} . Where $\boldsymbol{\varepsilon}$ and $\boldsymbol{\sigma}$ are the exact solution, and $\delta\hat{\boldsymbol{\varepsilon}}$ and $\delta\hat{\boldsymbol{\sigma}}$ are arbitrarily small errors.

Theorem 3

In the present SC-PIM, if

$$\delta^2\Pi(\mathbf{u})=\int_{\Omega}[-\delta\hat{\boldsymbol{\sigma}}^T\delta\hat{\boldsymbol{\varepsilon}}+2\delta\hat{\boldsymbol{\sigma}}^T\mathbf{L}_d\delta\mathbf{v}]d\Omega \tag{38}$$

is positive, then the strain energy obtained from SC-PIM solution is a lower bound of the exact solution in strain energy; if $\delta^2\Pi(\mathbf{v})<0$, the strain energy is a upper bound of the exact solution.

Proof

From Equation (21), total energy of SC-PIM can be written as

$$\begin{aligned} \hat{\Pi}(\mathbf{v}) &= \int_{\Omega} \left[-\frac{1}{2}(\boldsymbol{\sigma}+\delta\hat{\boldsymbol{\sigma}})^T(\boldsymbol{\varepsilon}+\delta\hat{\boldsymbol{\varepsilon}}) + (\boldsymbol{\sigma}+\delta\hat{\boldsymbol{\sigma}})^T\mathbf{L}_d(\mathbf{u}+\delta\mathbf{v}) \right] d\Omega - \int_{\Omega} \mathbf{b}^T(\mathbf{u}+\delta\mathbf{v}) d\Omega \\ &\quad - \int_{\Gamma_t} \mathbf{T}^T(\mathbf{u}+\delta\mathbf{v}) d\Gamma \\ &= \underbrace{\int_{\Omega} \left[-\frac{1}{2}\boldsymbol{\sigma}^T\boldsymbol{\varepsilon} + \boldsymbol{\sigma}^T\mathbf{L}_d\mathbf{u} \right] d\Omega - \int_{\Omega} \mathbf{b}^T\mathbf{u} d\Omega - \int_{\Gamma_t} \mathbf{T}^T\mathbf{u} d\Gamma}_{\Pi(\mathbf{u})} \\ &\quad + \underbrace{\int_{\Omega} [\delta\hat{\boldsymbol{\sigma}}^T(\mathbf{L}_d\mathbf{u}-\hat{\boldsymbol{\varepsilon}}) - (\mathbf{L}_d^T\hat{\boldsymbol{\sigma}})^T\delta\mathbf{v} - \mathbf{b}^T\delta\mathbf{v}] d\Omega}_{\delta\Pi(\mathbf{u})} \\ &\quad + \frac{1}{2} \underbrace{\int_{\Omega} [-\delta\hat{\boldsymbol{\sigma}}^T\delta\hat{\boldsymbol{\varepsilon}} + 2\delta\hat{\boldsymbol{\sigma}}^T\mathbf{L}_d\delta\mathbf{v}] d\Omega}_{\delta^2\Pi(\mathbf{u})} \end{aligned} \tag{39}$$

where

$$\delta\Pi(\mathbf{u})=\int_{\Omega}[\delta\hat{\boldsymbol{\sigma}}^T(\mathbf{L}_d\mathbf{u}-\hat{\boldsymbol{\varepsilon}})-(\mathbf{L}_d^T\hat{\boldsymbol{\sigma}})^T\delta\mathbf{v}-\mathbf{b}^T\delta\mathbf{v}]d\Omega \tag{40}$$

and $\delta^2\Pi(\mathbf{u})$ is shown in Equation (38).

In deriving Equation (39), we have used the fact that $\delta\mathbf{v}=0$ on Γ_u . The stationary condition $\delta\Pi=0$ indicates that $\hat{\Pi}(\mathbf{u}+\delta\mathbf{v})>\Pi(\mathbf{u})$ if $\delta^2\Pi(\mathbf{u})>0$ and $\hat{\Pi}(\mathbf{u}+\delta\mathbf{v})<\Pi(\mathbf{u})$ when $\delta^2\Pi(\mathbf{u})<0$.

In addition, the total potential energy in the discrete form at the stationary point is

$$\hat{\Pi}(\hat{\mathbf{d}})=\frac{1}{2}\hat{\mathbf{d}}^T\hat{\mathbf{K}}\hat{\mathbf{d}}-\hat{\mathbf{d}}^T\mathbf{f}=-\frac{1}{2}\hat{\mathbf{d}}^T\hat{\mathbf{K}}\hat{\mathbf{d}}=-\hat{U}(\hat{\mathbf{d}}) \tag{41}$$

Hence when $\delta^2\Pi(\mathbf{u})>0$, we have $-\hat{U}(\hat{\mathbf{d}})\geq-U(\mathbf{d})$ or $\hat{U}(\hat{\mathbf{d}})\leq U(\mathbf{d})$, which means that the strain energy is a lower bound of the exact solution. If $\delta^2\Pi(\mathbf{u})<0$ holds, we then have $-\hat{U}(\hat{\mathbf{d}})\leq-U(\mathbf{d})$

or $\hat{U}(\hat{\mathbf{d}}) \geq U(\mathbf{d})$, which shows that strain energy is an upper bound of the exact solution. This completes the proof. \square

Corollary 2

In SC-PIM, we now define

$$\begin{aligned} \pi(\hat{\mathbf{u}}; \alpha) = & \sum_{k=1}^N \sum_{i=1}^M \int_{\Omega_{k,i}} A_{k,i} [-(3+2\alpha+\alpha^2)(\delta\tilde{\mathbf{e}}_k^T \mathbf{D} \delta\tilde{\mathbf{e}}_k \\ & + \delta\tilde{\mathbf{e}}_{k,i}^T \mathbf{D} \delta\tilde{\mathbf{e}}_{k,i} - 2\delta\tilde{\mathbf{e}}_k^T \mathbf{D} \delta\tilde{\mathbf{e}}_{k,i}) + 6\delta\tilde{\mathbf{e}}_{k,i}^T \mathbf{D} \delta\tilde{\mathbf{e}}_{k,i}] d\Omega \end{aligned} \quad (42)$$

If $\pi(\hat{\mathbf{u}}; \alpha) > 0$, the strain energy for SC-PIM is a lower bound of the exact solution; if $\pi(\hat{\mathbf{u}}; \alpha) < 0$, the strain energy is an upper bound of the exact solution.

Corollary 2 is the results of Equations (31), (32), (38) and Theorem 3.

Note that due to the smoothing operation, the assumed strains $\tilde{\mathbf{e}}_k$ from LC-PIM is constant in each smoothing domain Ω_k . Therefore, we have

$$\int_{\Omega_k} \delta\tilde{\mathbf{e}}_k^T \mathbf{D} \delta\tilde{\mathbf{e}}_{k,i} d\Omega = \int_{\Omega_k} \delta(\mathbf{L}_d^T \tilde{\mathbf{e}}_k)^T \mathbf{D} \delta\tilde{\mathbf{u}}_{k,i} d\Omega = 0 \quad (43)$$

Corollary 3

The SC-PIM produces a lower bound solution when $\alpha=0$.

This can be shown easily by invoking $\alpha=0$ in Equation (42), which gives

$$\pi(\hat{\mathbf{u}}; \alpha) = 3 \sum_{k=1}^N \left[\sum_{i=1}^M (A_{k,i} \delta\tilde{\mathbf{e}}_{k,i}^T \mathbf{D} \delta\tilde{\mathbf{e}}_{k,i}) - A_k \delta\tilde{\mathbf{e}}_k^T \mathbf{D} \delta\tilde{\mathbf{e}}_k \right] > 0 \quad (44)$$

This means that the SC-PIM produces a lower bound solution.

Corollary 4

The SC-PIM produces an upper bound solution when $\alpha=1$.

This can be shown also easily by invoking $\alpha=1$ in Equation (42), which gives

$$\pi(\hat{\mathbf{u}}; \alpha) = \sum_{k=1}^N \sum_{i=1}^M -6A_{k,i} \delta\tilde{\mathbf{e}}_k^T \mathbf{D} \delta\tilde{\mathbf{e}}_k < 0 \quad (45)$$

This means that the SC-PIM produces an upper bound solution.

Note that the SC-PIM solution with $\alpha=1$ is in fact the LC-PIM solution.

Note that there will be cases for which Corollary 4 is not true, when only a few linear elements are used as reported in the LC-PIM model [21]. This is because we need the SC-PIM model is reasonably fine so that $\delta\mathbf{v}$ is a small variation near the exact solution. In the cases with a few elements, the numerical solutions may be far away from the exact solution and hence the variation $\delta\mathbf{v}$ is not small; hence, Theorem 3 fails for these cases.

Note also that the bound property of SC-PIM also depends on the smoothing effect. This can be clearly seen from Equation (38), where $\hat{\mathbf{e}}$ and hence $\hat{\mathbf{c}}$ all depend on the how the smoothing is performed and the dimension of the smoothing domains. Figure 3 shows a simple example of energy potential surface obtained using a 1D problem of a uniform bar subjected to a uniformly

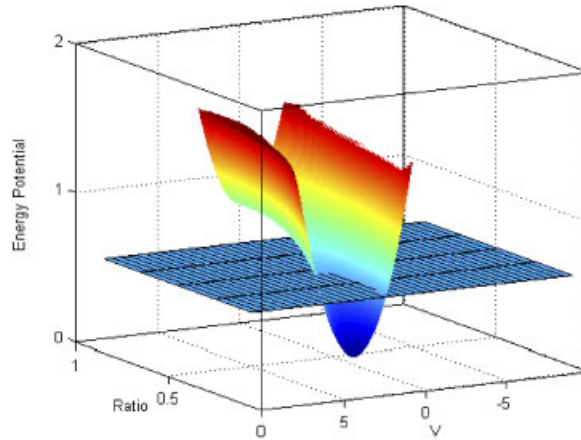


Figure 3. A simple example of energy potential surface obtained using a 1D problem of a uniform bar subjected to a uniformly distributed force. The 'ratio' denotes the ratio of the smoothing domain in relation to the whole domain; the flat plane is the exact solution. The valley of the surface is the trace of the SC-PIM solution varying with the ratio of the smoothing domain. It is clear that the upper bound solution occurs with an increase of smoothed domain.

distributed force (see Section 8.2 for detailed description on the problem). In producing Figure 3, we use only two linear elements with three nodes. We then fix the two end-nodes so that the displacement field can be controlled only by the middle node. The smoothing operation is only applied to the middle node symmetrically, and the dimension of the smoothing domain is varied. The 'ratio' denotes the ratio of the smoothing domain in relation to the whole domain of the bar; the flat plane denotes the exact solution. The valley of the surface is the trace of the SC-PIM solution varying with the ratio of the smoothing domain. It is clear that the upper bound solution occurs with an increase of smoothed domain.

The smoothing effect is also related to density of the mesh used in SC-PIM. Eventually, whether or not a method can produce an upper bound solution depends on the battle between the stiffening effect induced by the assumption of the displacement field and the softening effect provided by the smoothing operation. Detailed discussions on this can be found in [21, 30].

7. SUPERCONVERGENCE OF THE SC-PIM AND DETERMINATION OF PREFERABLE α

In the error analysis for FEM [24, 31] based on the minimum total potential principle, the determination of the upper bound of $\|u - u_h\|_m$ is usually reduced to the estimation of $\|u - \Pi_h u\|_m$. By the approximation theory, we can only obtain, limited by the degree n of the approximation polynomials, that

$$\|\mathbf{u} - \Pi_h \mathbf{u}\|_m \leq Ch^{n+1-m} \|\mathbf{u}\|_{n+1} \quad (46)$$

In general this estimate cannot be improved even if the solution \mathbf{u} possesses a higher smoothness. Therefore,

$$\|\mathbf{u} - \Pi_h \mathbf{u}\|_m = O(h^{n+1-m}) \quad (47)$$

is the *optimal* order error estimate. By ‘optimal’ we mean that the rate of convergence *cannot* be improved, and the rates are also called theoretical rates. For linear FEM, the optimal theoretical rate is 2.0 for the displacement norm and 1.0 for the strain energy norm. It is known that this fact does not exclude the possibility that the approximation of the derivatives may be of higher-order accuracy at some special points, called superconvergence points. This means that one can find points in the elements, where the rate of convergence for the strain energy is more than 1.0 and less than 2.0. However, for the displacement, the theoretical value of 2.0 still cannot be improved.

We will show in Section 8 that the SC-PIM has a special superconvergent property that behaves very differently from the fully compatible FEM models. The SC-PIM is equipped with an adjustable parameter α . Both the displacement field $\hat{\mathbf{u}}(\alpha)$ and strain field $\hat{\boldsymbol{\varepsilon}} = (\hat{\mathbf{u}}(\alpha); \alpha)$ are the functions of α . Therefore, an adjustment on α can obviously influence the accuracy and convergence of solutions in *both* displacement and strain energy norms. When α is properly tuned, the SC-PIM can produce a convergence rate that far exceeds the so-called theoretical optimal values for in both measures of displacement and strain energy norms: a truly superconvergence.

Furthermore, Section 6 has proven that the solution of the SC-PIM with $\alpha=0$ is a lower bound of the exact solution in energy norm; whereas for $\alpha=1$, it is an upper bound. Thus, there must exist a value $\alpha_{\text{exact}} \in (0, 1)$ at which the strain energy is the exact solution. This implies that we should be able to obtain the ‘exact’ solution using an SC-PIM model of finite dimension! Therefore, the rate of convergence in energy norm can be, in theory, infinite. This opens an opportunities for establishing extremely fast convergence models producing ultra accurate solutions, even liner field is used.

Finding such an ‘exact’ α is ideal, but requires extra efforts. Our study has found that such an α_{exact} is, unfortunately, in general problem-dependent and also mesh-dependent. Hence it requires a number of trials-of-error to find an ideal α that is very close to the α_{exact} for a given problem, unless a universally workable ‘magic’ formula can be found. Fortunately, when one only wants to find a ‘preferable’ α that gives a ‘good’ superconvergent solution, the following simple ways are recommended.

(1) Simply use $\alpha=0$. This is effortless, and it will produce superconvergent solution that is much more (often more than 10 times!) accurate than either FEM or LC-PIM using the same mesh, as shown in all the example problems in this paper.

(2) Our intensive study using numerical examples has discovered an important fact that the α_{exact} is approximately a linear function of the mesh size h for a given model of a problem. We can therefore assume

$$\alpha_{\text{exact}}(h) \approx \alpha_{\text{pref}}(h) = \beta_h + \gamma \quad (48)$$

where β and γ are unknown and problem-dependent constants. This discovery leads to a simple curve-fitting method to find a preferable $\alpha_{\text{pref}}(h)$ that is very close to the α_{exact} for a given problem:

- (i) Create a model $M^{(1)}$ with a coarse mesh, and slightly finer model $M^{(2)}$ with elements of the same aspect ratio as model $M^{(1)}$. The nodal spacing of the $M^{(1)}$ and $M^{(2)}$ is denoted as h_1 .
- (ii) Use $M^{(1)}$ and $M^{(2)}$ to compute two $\hat{U}^{(1)}(\alpha) \sim \alpha$ and $\hat{U}^{(2)}(\alpha) \sim \alpha$ curves using Equations (28) and (32).
- (iii) Obtain the intersection point $\alpha^{(1)}(h_1)$ of these two curves.

- (iv) Use procedures defined in (i)–(iii) again to compute another $\alpha^{(2)}(h_2)$ using $M^{(2)}$ and other model $M^{(3)}$ that is slightly finer than $M^{(2)}$ but with the same aspect ratio. The average nodal spacing for these two models is denoted as h_2 .
- (v) The unknown β and γ in Equation (48) can now determined using

$$\beta = \frac{\alpha^{(1)}(h_1) - \alpha^{(2)}(h_2)}{h_1 - h_2} \quad \text{and} \quad \gamma = \alpha^{(1)}(h_1) - \beta h_1 \quad (49)$$

Using above the procedure, we can now obtain a preferable $\alpha_{\text{pref}}(h)$ that should works very well for all meshes of the same aspect ratio for the given problem. When such a ‘preferable’ α is found, the superconvergent solution can be obtained for both the strain energy and the displacement.

Equation (48) effectively resolves (to certain extend) the issue of dependence of α on the mesh, and $\alpha_{\text{pref}}(h)$ is now only problem depend. Note that Equation (48) may not be the best formula, but it reveals an important insight: if the assumed strain field can be tuned taking the characteristics of the mesh h into account, we can then achieve a ‘shortcut’ to arrive right at the exact solution.

8. NUMERICAL EXAMPLES AND DISCUSSIONS

In this section, a number of numerical examples will be examined using the SC-PIM with both linear and quadratic interpolation. To investigate quantitatively the numerical results, the error indicators in both displacement and energy norms are defined as follows:

$$E_d = \sqrt{\frac{\sum_{i=1}^n (u_i^{\text{ref}} - u_i^{\text{num}})^2}{\sum_{i=1}^n (u_i^{\text{ref}})^2}} \quad (50)$$

$$E_e = \sqrt{\frac{|U_{\text{num}} - U_{\text{ref}}|}{U_{\text{ref}}}} \quad (51)$$

where the superscript ref denotes the reference or analytical solution, num denotes a numerical solution obtained using a numerical method.

8.1. Standard path test

For a numerical method working for solid mechanics problems, the sufficient requirement for convergence is to pass the standard path test [23]. Therefore, the first example is the standard path test using the present SC-PIM. A rectangular patch of 10×50 is considered, and the displacements are prescribed on all outside boundaries by the following linear function:

$$\begin{aligned} u_x &= 0.6x \\ u_y &= 0.6y \end{aligned} \quad (52)$$

The patch is represented using nodes shown in Figure 4. All the error for any $\alpha \in [0, 1]$ in displacement norm defined in Equation (50) are found less than 1.0×10^{-14} . This example demonstrates numerically that the SC-PIM can pass the standard path test and is at least linearly conforming.

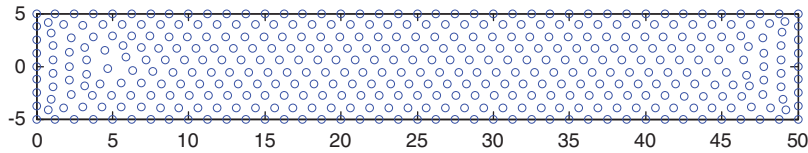


Figure 4. Node distributions for the standard patch test.

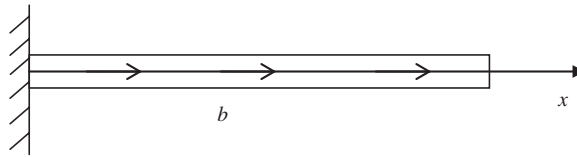


Figure 5. One-dimensional bar subjected to a uniformly distribute body force.

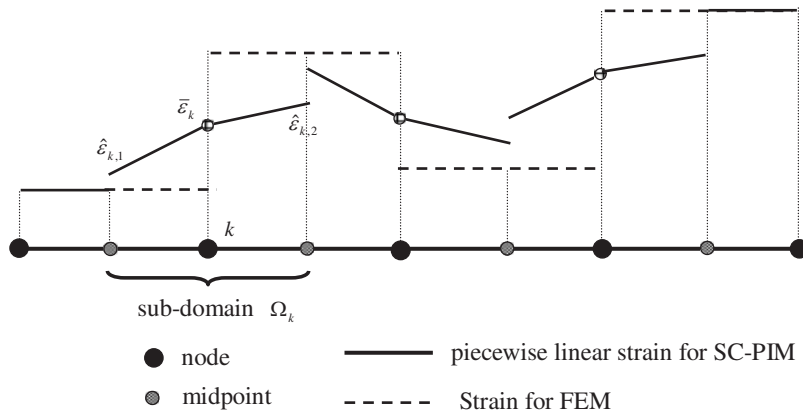


Figure 6. Strain field assumed in SC-PIM for 1D bar.

8.2. One-dimensional bar problem

Consider first a simple problem of a bar with length L and uniform cross-sectional area A , as shown in Figure 5. The bar is fixed at the left end and subjected to a uniform body force b . The parameters are taken as $L = 1 \text{ m}$, $A = 1 \text{ m}^2$, $b = 1 \text{ N/m}$ and $E = 1.0 \text{ Pa}$. The strain field assumed in SC-PIM is illustrated in Figure 6.

The governing equation and boundary conditions of the 1D bar problem should be

$$E \frac{d^2 u}{dx^2} + 1 = 0 \tag{53}$$

$$u|_{x=0} = 0, \quad \sigma|_{x=1} = 0$$

The analytical solution that satisfies the above equations is obtained as

$$u(x) = -\frac{1}{2E}x^2 + \frac{1}{E}x \quad (54)$$

To study the convergence property of the SC-PIM solution for 1D bar problem, the model with regularly distributed nodes has been analyzed. First, the strain energy of SC-PIM with linear displacement field for different parameter α is calculated and plotted in Figure 7. It is found that SC-PIM has upper and lower bound solutions of the exact solution when $\alpha = 0.5$ and 0.009, respectively. Furthermore, the strain energy for these model lies in between those from the compatible FEM solution and the LC-PIM solution that is the same as SC-PIM with $\alpha = 1$. These findings verify Theorem 2.

Using Equations (50) and (51), errors in displacement and energy norms are computed and plotted against the average nodal spacing (h) as shown in Figures 8 and 9. It is clear that when $\alpha = 1, 0.5$ and 0.009, the convergence rate in displacement norm is about 2, which is similar to that of the linear FEM. However, when $\alpha = 0$ and 0.009, the convergence rates in energy norm are approximately 1.48 and 1.98, which are obviously much higher than the theoretical value of 1.0. Hence, using SC-PIM we have obtained a much higher than usual convergence rate in energy norm: superconvergence. Note also that the theoretical *optimal* value for energy norm is 1.0. The SC-PIM with $\alpha = 0.009$ has achieved 1.98, which is indeed remarkable.

8.3. Cantilever 2D solid

A 2D cantilever solid is now studied as shown in Figure 10. The solid is subjected to a parabolic traction at the free end, and the analytical solutions can be found in Reference [32].

To study the convergence property, the strain energy of SC-PIM with linear displacement field for different α is computed and plotted in Figure 11. It is easy to see that SC-PIM has upper and lower bound solutions when $\alpha = 0.9, 0.14$ and 0. Furthermore, the strain energy for this model is

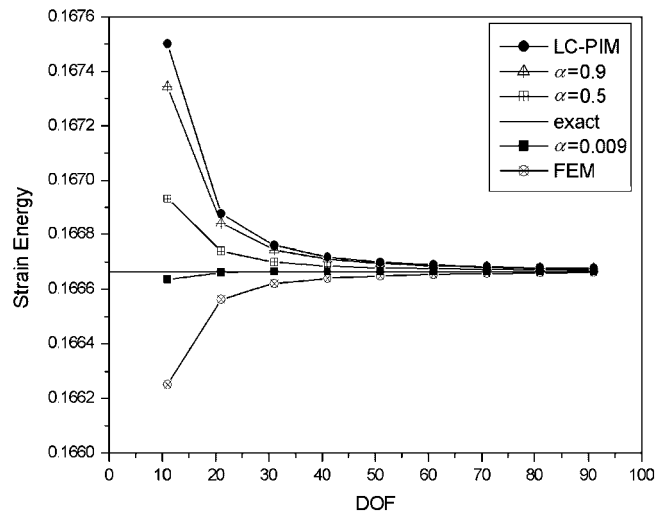


Figure 7. Solution in strain energy of the SC-PIM for 1D bar problem.

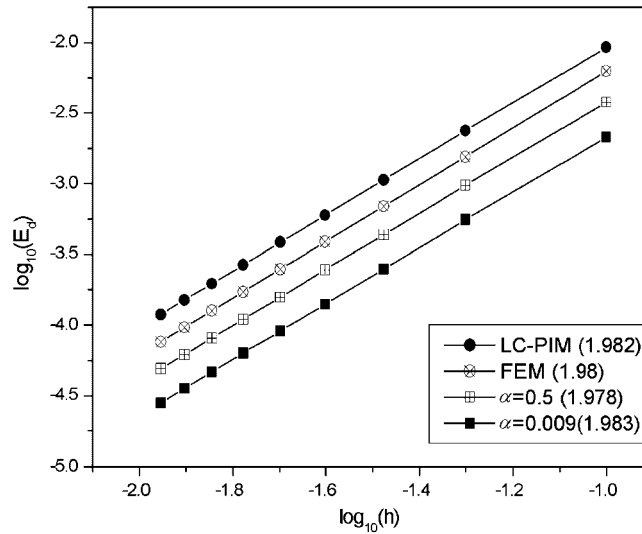


Figure 8. Convergence of the SC-PIM solution in displacement norm for 1D bar problem.

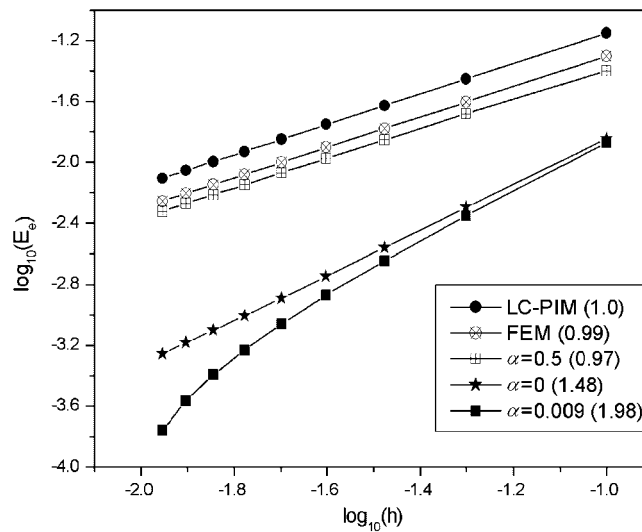


Figure 9. Convergence of the SC-PIM solution in energy norm for 1D bar problem.

no-less than that from the compatible FEM solution, and no-larger than the strain potential from the LC-PIM solution. These findings verify again Theorem 2.

Using Equation (50), error in displacement norm is computed and plotted in Figure 12. When $\alpha=0$ and 0.14, the convergence rates in displacement norm are, respectively, about 2.36 and 3.79, which are much higher even than that of 4-node FEM, and the theoretical value of 2.0. This shows that we achieved superconvergence in *displacement* solution, which is not possible in the

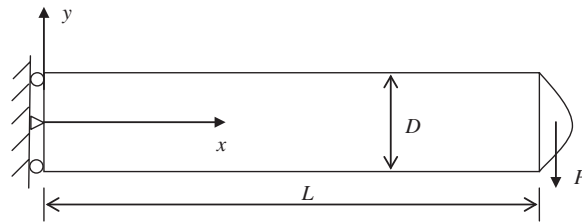


Figure 10. A 2D cantilever solid subjected to a parabolic traction on the right edge.

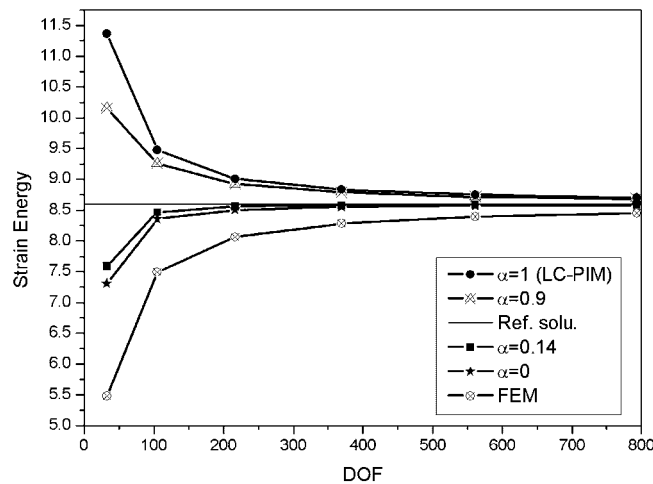


Figure 11. Upper and lower bound solutions of the SC-PIM for 2D beam.

standard FEM models. We then compute α_{pref} using the procedures detailed in Section 7 and found $\alpha_{\text{pref}}(h) = 0.101h + 0.122$. The convergence rate of SC-PIM in displacement norm is about 2.98 when $\alpha = \alpha_{\text{pref}}(h)$, which is also much higher than theoretical ‘optimal’ value.

Using Equation (51), error in energy norm is computed and plotted in Figure 13. It is found that the convergence rates in energy norm are, respectively, 1.15, 2.05 and 1.62 when $\alpha = 0, 0.14$ and $\alpha_{\text{pref}}(h) = 0.101h + 0.122$, which is obviously much higher than that of the FEM of 3-node and even 4-node elements and the theoretical value of 1.0.

These examples show clearly the very high accuracy of the solution and excellent superconvergence property of the SC-PIM.

8.4. Infinite 2D solid with a circular hole

An infinite 2D solid with a central circular hole and subjected to a unidirectional tensile is studied. Owing to its two-fold symmetry, one quarter is modeled as shown in Figure 14. Symmetry conditions are imposed on the left and bottom edges, and the inner boundary of the hole is traction free. The analytical solution of this benchmark problem can be found in Reference [32].

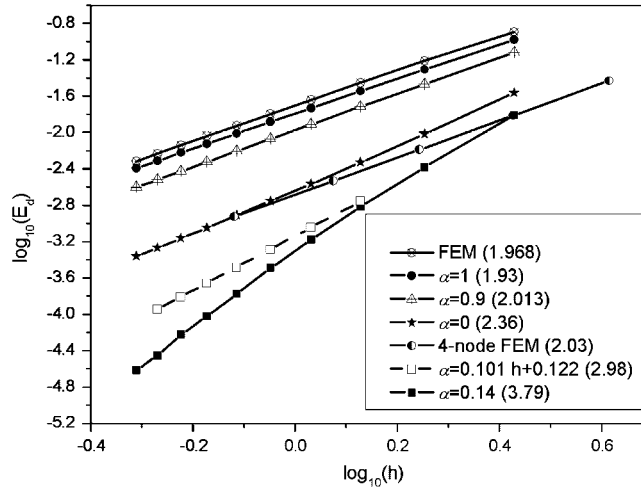


Figure 12. Convergence of the SC-PIM solution in displacement norm for different α . The dashed line is obtained from SC-PIM solution with α_{pref} using the procedure given in Section 7. It is clear that the SC-PIM with α_{pref} is of superconvergence of high rate.

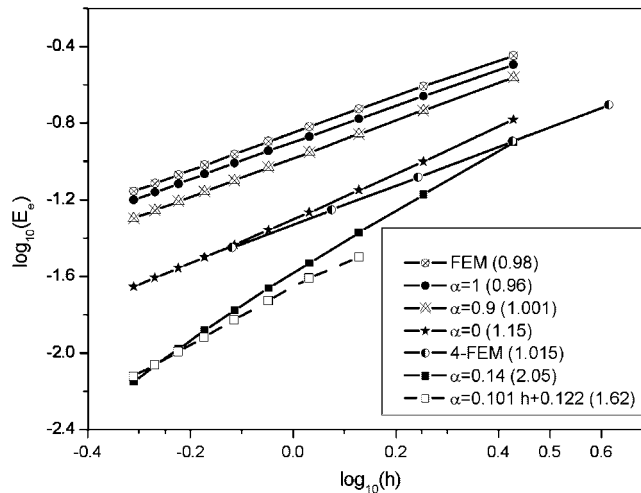


Figure 13. Convergence of the SC-PIM solution in energy norm for different α . The dashed line is obtained from SC-PIM solution with α_{pref} using the procedure of Section 7. It is clear that the SC-PIM with α_{pref} is of superconvergence of high rate.

To study the convergence property, the strain energy of the SC-PIM with linear displacement field for different parameter α is computed and plotted in Figure 15. It is easy to see that SC-PIM has upper and lower bounds solutions of the exact solution when $\alpha = 0.9, 0.475$ and 0 , respectively. Furthermore, the strain energy for these model is no-less than that from the compatible FEM solution, and no-larger than the strain potential from the LC-PIM solution.

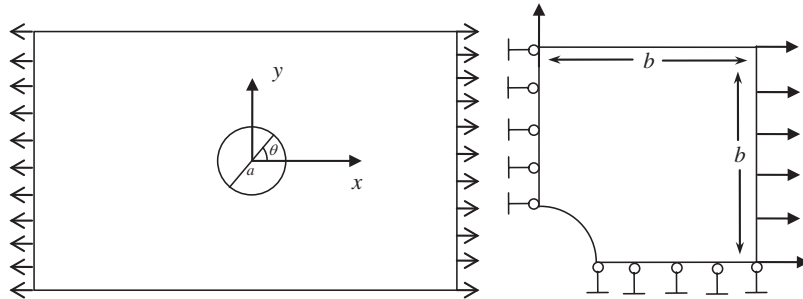


Figure 14. Infinite 2D solid with a hole subjected to a tensile force and its quarter model.

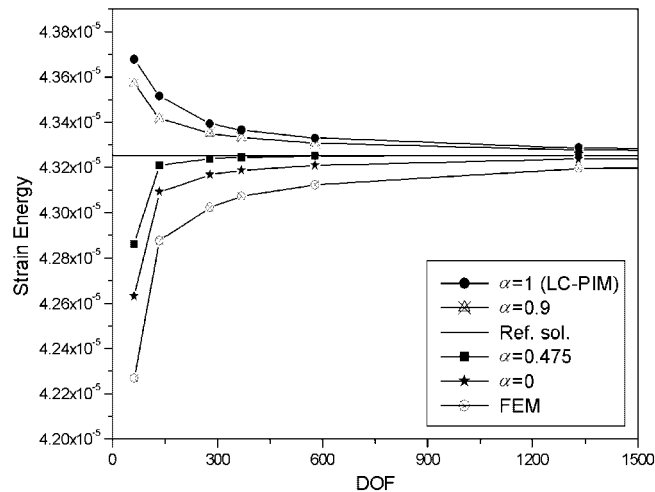


Figure 15. Lower and upper bound solutions of the SC-PIM for 2D solid with hole.

Using Equations (50) and (51), errors in displacement and energy norms are computed and plotted against the average nodal spacing (h) as shown in Figures 16 and 17. It is clear that when $\alpha=0.475$ the convergence rates in displacement and energy norms are, respectively, about 2.49 and 2.149, which clearly show the superconvergence both the displacement and the energy norms.

We compute α_{pref} using the procedures detailed in Section 7 and found $\alpha_{\text{pref}}(h) = 0.574h + 0.415$. The convergence rates in displacement norm and energy norm are, respectively, about 2.17 and 1.92 when $\alpha = \alpha_{\text{pref}}(h)$, which clearly show again the superconvergence for the strain energy.

8.5. Semi-infinite plate

A two-dimensional half space subjected to a uniform pressure on the upper surface within a finite range is studied (see Figure 18). Plane strain condition is considered and the analytical solutions can be found in Reference [32].

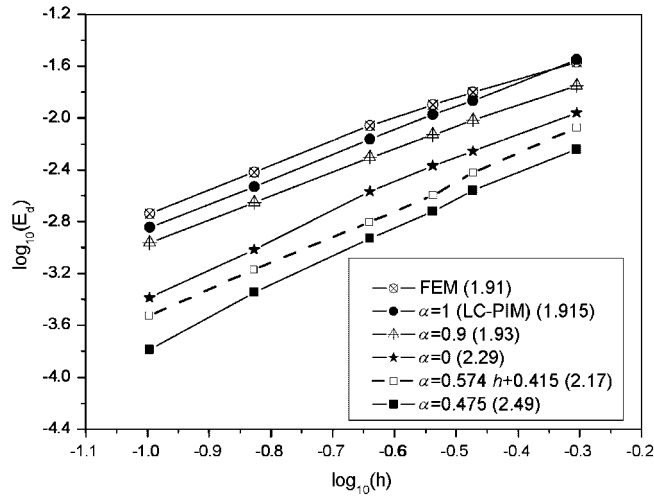


Figure 16. Convergence of the SC-PIM in displacement norm for 2D solid with hole. The dashed line is obtained from SC-PIM solution with approximation of α using the procedure of Section 7. It is clear that the SC-PIM with α_{pref} is of superconvergence.

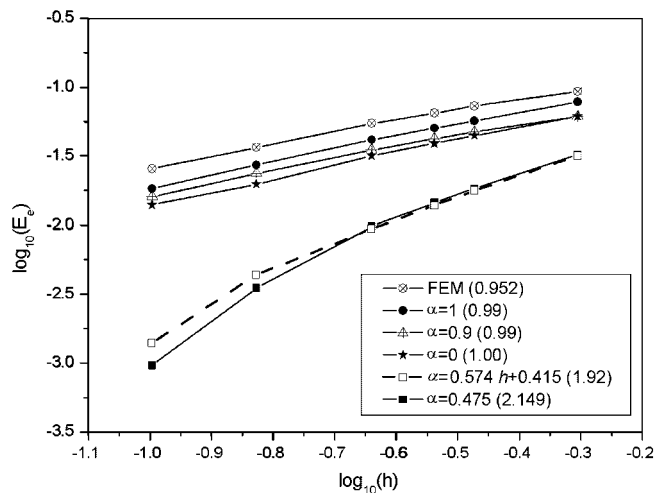


Figure 17. Convergence of the SC-PIM in energy norm for 2D solid with hole. The dashed line is obtained from SC-PIM solution with α_{pref} using the procedure in Section 7. It is clear that the SC-PIM with α_{pref} is of superconvergence.

To study the convergence property of the SC-PIM solution, the strain energy for SC-PIM with linear displacement field for different α is calculated and plotted in Figure 19. It is easy to see that SC-PIM has upper and lower bound solutions of the exact solution when $\alpha=0.9, 0.4375$ and 0 , respectively. Furthermore, the strain energy for this model is no-less than that from the compatible FEM solution, and no-larger than the strain potential from the LC-PIM. Using Equations (50) and

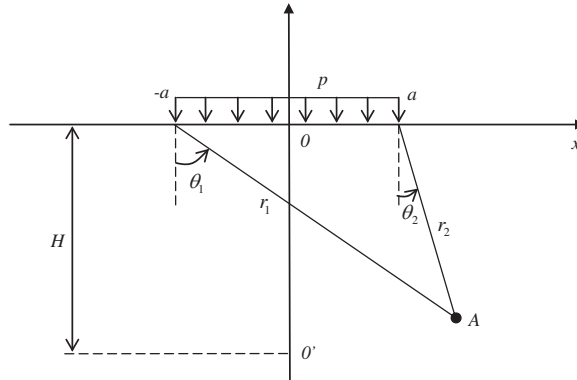


Figure 18. Semi-infinite 2D solid subjected to a uniform pressure on the surface.

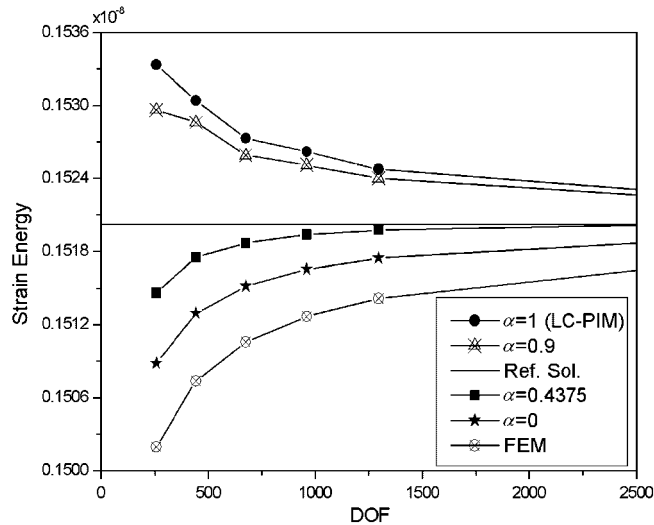


Figure 19. Solution in strain energy of the SC-PIM for different α .

(51), errors in displacement and energy norms are calculated and plotted in Figures 20 and 21. It can be found that the convergence rate in displacement norm for the SC-PIM with different α is very similar to that of the FEM solution. However, the convergence rate in energy norm for SC-PIM with $\alpha=0.4375$ is about 1.63 and is much higher than usual one in energy norm, which clearly shows the superconvergence in energy norm.

8.6. Square solid subjected to uniform pressure and body force

A square solid that is considered as plane stress is now studied as shown in Figure 22. The solids are constrained on the left, the right, and the bottom edges, and suffering from uniform pressure along the top edge and body force.

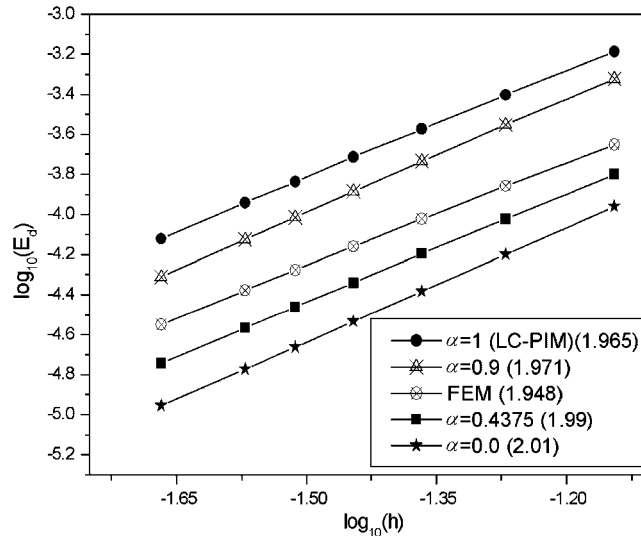


Figure 20. Convergence of the SC-PIM solution in displacement norm for different α .

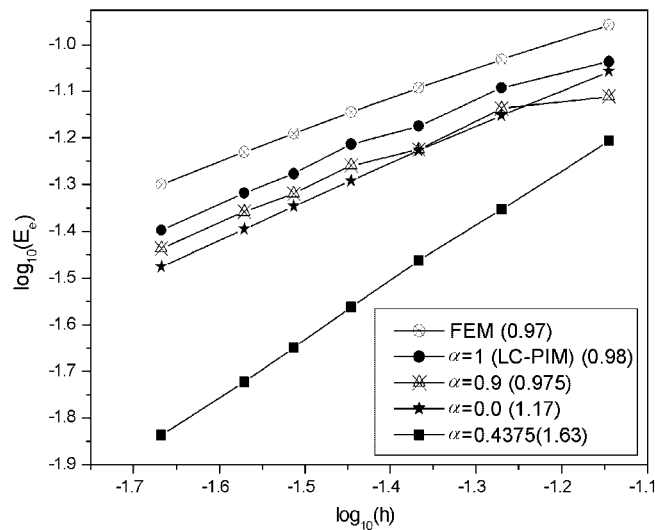


Figure 21. Convergence of the SC-PIM solution in energy norm for different α .

The convergence property and energy bound for SC-PIM are also investigated in similar manners as in the previous examples. As the analytical solution is not available for this problem, the reference solution of strain energy is obtained using the FEM with a very fine mesh (8238 nodes). The computed strain energy and convergent rate in energy norm for different α are plotted in Figures 23 and 24, respectively. It is easy to see that using SC-PIM we have also obtained the higher convergence rate in energy norm.

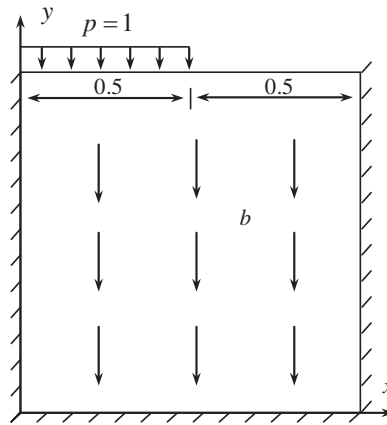


Figure 22. A square solid with body force subjected to a uniform pressure.

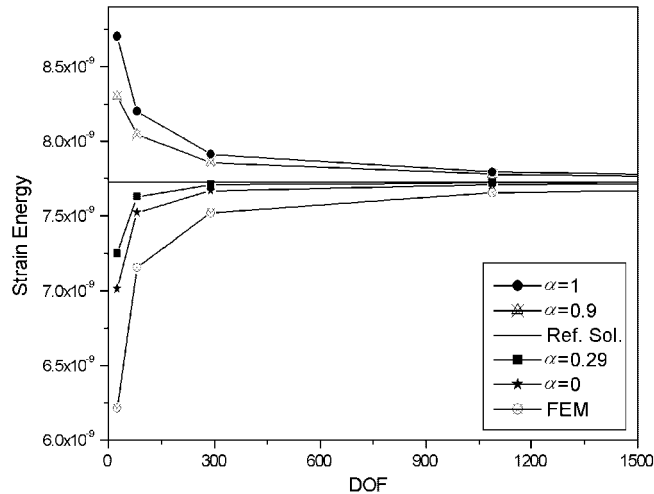


Figure 23. Upper and lower bound solution of the SC-PIM for different α .

8.7. SC-PIM with high-order polynomials interpolation

We now examine the 2D cantilever beam using SC-PIM with quadratic polynomials interpolation. The details on construction of quadratic PIM shape function based on triangular cells can be found in Reference [16]. To study the convergence property of the SC-PIM solution with quadratic interpolation, the strain energy of SC-PIM for different α is calculated in Figure 25. It is clearly seen that SC-PIM produces upper bound solutions of the exact solution when $\alpha=1.0$ and 0.9 , and lower bound solutions when $\alpha=0.325$ and 0 . Using Equations (50) and (51), errors in displacement and energy norms are calculated and plotted in Figures 26 and 27. From these figures, it is easy to see that when $\alpha=0$ and 0.325 , the accuracy and convergence rates in displacement norm and energy norm are very high, which show again that SC-PIM is of superconvergence.

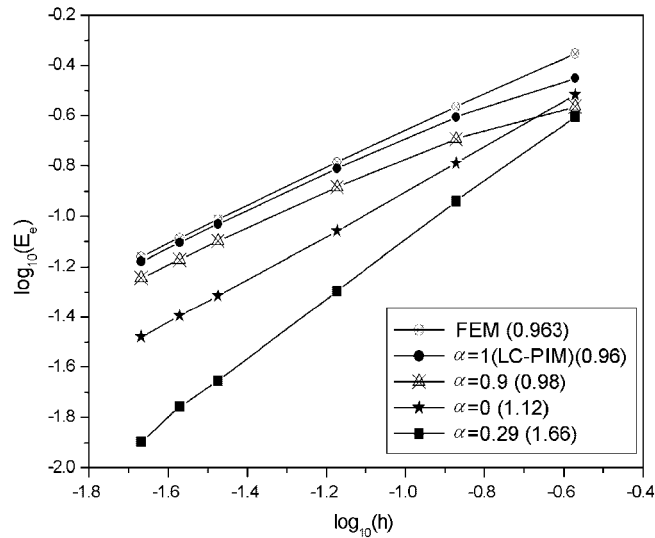


Figure 24. Convergence of the SC-PIM in energy norm for different α .

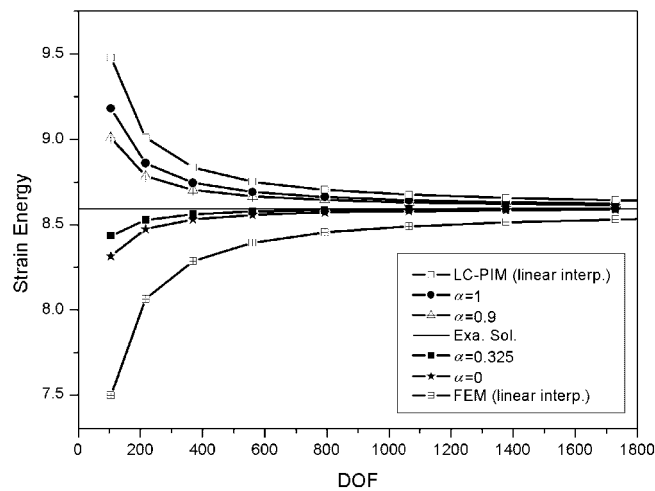


Figure 25. The upper and lower bounds solution of strain energy for different α used in SC-PIM with quadratic interpolation.

8.8. Discussions on the computational efficiency of SC-PIM

Corollary 1 in Section 5 shows that the stiffness matrix $\hat{\mathbf{K}}$ obtained using SC-PIM is symmetrical and has the same dimension when the same mesh and node number system are used. This is because SC-PIM has not introduced any extra unknown variables compared with the FEM. Considering the extra computing cost in computing the strain field for establishing the stiffness matrix, SC-PIM will take more computation time compared with the FEM of the same mesh. However, when

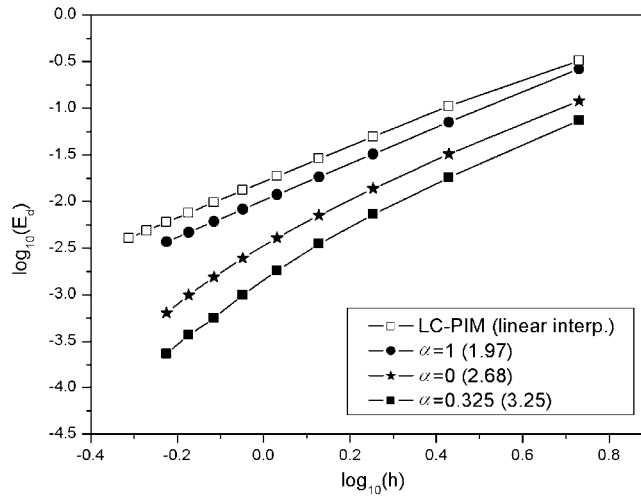


Figure 26. Convergence of SC-PIM solution in displacement norm for different α used in SC-PIM with quadratic interpolation.

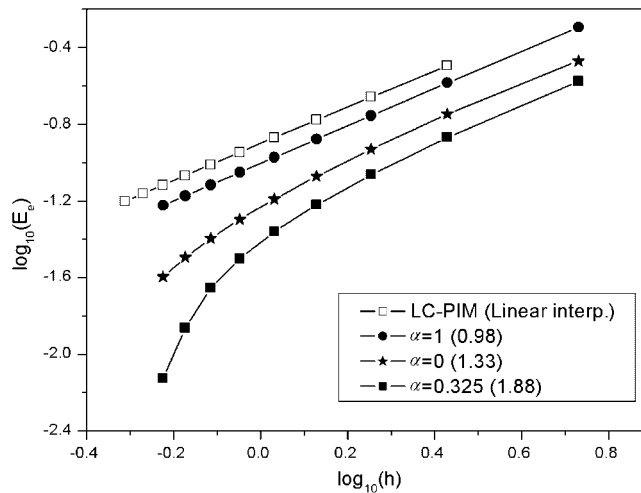


Figure 27. Convergence of SC-PIM solution in energy norm for different α used in SC-PIM with quadratic interpolation.

an iterative solver is used, the SC-PIM equations can be solved more efficiently because of the better conditioning in $\hat{\mathbf{K}}$ due to the softening effects. Furthermore, the much higher accuracy and convergence of SC-PIM will result in a higher computational efficiency compared with the FEM.

To confirm this numerically, we test the CPU time for both SC-PIM and FEM using the cantilever example with 10×50 mesh detailed in Section 8.3. It has been found that the CPU time used in SC-PIM is 1.47 s, which is approximately more than 8.8% than that of FEM (1.35 s), when the

same equation solver is used. It confirms that the computational cost of SC-PIM is almost the same as that of FEM when same mesh is used.

For a fairer comparison, we now produce the efficient curve: CPU time taken for the solution of same accuracy. Figures 28 and 29 plot, respectively, the energy and displacement errors obtained against the CPU times used by FEM, LC-PIM and SC-PIM with different α . It is clear that for the same CPU time SC-PIM can obtain solution of higher accuracy, and for the same accuracy in solution, SC-PIM needs less CPU times compare with the FEM for all the α used. When a 'preferable' α is used, the accuracy of the SC-PIM can be more than 10 times of that of the FEM when the same CPU time is used.

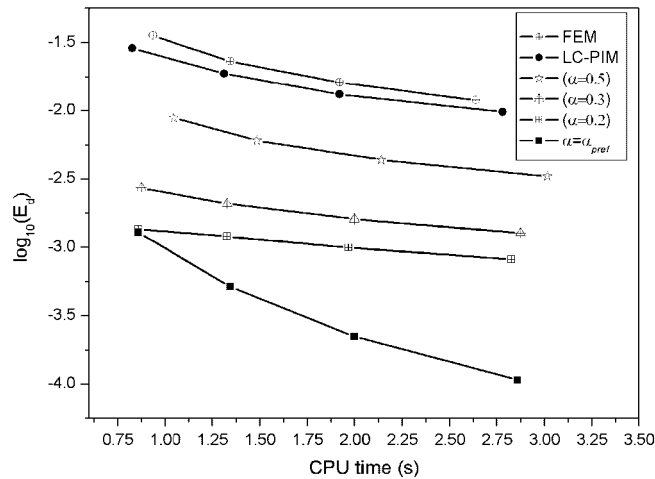


Figure 28. Comparison of efficiency between FEM, LC-PIM and SC-PIM in displacement norm.

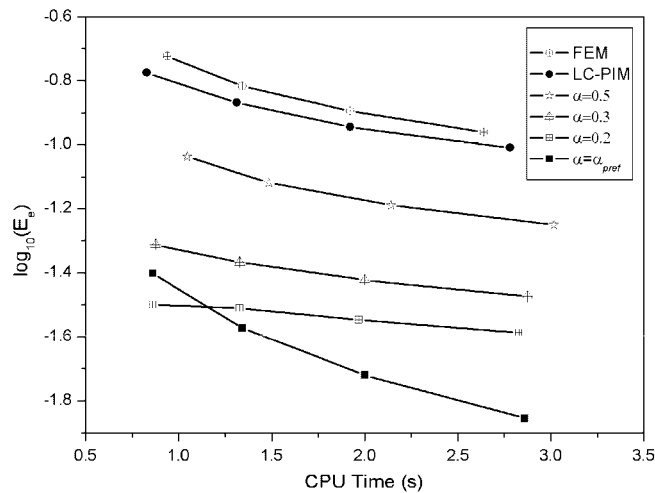


Figure 29. Comparison of efficiency between FEM, LC-PIM and SC-PIM in energy norm.

9. CONCLUSIONS

In this work, an SC-PIM with piecewise linear strain field is proposed by combining the techniques of the FEM and the LC-PIM using triangular meshes. We proved theoretically (1) when the same mesh is used, the strain energy obtained from the SC-PIM solution is no-less than that from the compatible FEM solution and no-larger than the strain potential for the LC-PIM model; (2) the exact solution is bounded by those of SC-PIM with $\alpha = 1$ from above and $\alpha = 0$ from below; (3) there exists an α at which the SC-PIM gives the exact solution in energy norm. Finally, a practical procedure is presented to find an $\alpha_{\text{pref}}(h)$ that gives very accurate solution with superconvergence. Intensive numerical studies verified the convergence, superconvergence and bounds property of the SC-PIM:

- (1) Higher accurate solution and convergence rates in both displacement and energy norm can be obtained using the SC-PIM.
- (2) For the properly chosen α , PIM-CSS can produce upper bound, lower bound and even the superconvergent solution, which shows that the α can be used as a adjustor to provide the 'softer' or 'stiffer' effects to system.
- (3) Although triangular elements are used in SC-PIM, it can produce much better solution than that of the quadrilateral elements of FEM.
- (4) The SC-PIM is superconvergent for any $\alpha \in (0, 1)$; and corresponding strain and stress solutions are piecewise linear in any smoothing domain; SC-PIM with $\alpha = 0$ is simple, works for all the problems studied, gives very accurate solution of superconvergence, and hence is recommended. Even better solution can be obtained using α_{pref} that requires additional cost in determining α_{pref} for a given problem. It is possible to build an even better shortcut to attain the exact solution.

Finally, we note that the discussion of this paper focuses on energy norms as a global measure. Other norm measures should be possible. In fact, an extension to any other *equivalent* norms should be straightforward.

ACKNOWLEDGEMENTS

This work was supported in part by the National Natural Science Foundation of China under Grants 10532050, 10501017, 60673023, and by the 985 program of Jilin University, China. The authors also thank the support of Centre for ACES and Singapore-MIT Alliance (SMA), National University of Singapore.

REFERENCES

1. Lucy LB. A numerical approach to testing the fission hypothesis. *The Astronomical Journal* 1977; **8**(12): 1013–1024.
2. Liu GR, Liu MB. *Smoothed Particle Hydrodynamics—A Meshfree Practical Method*. World Scientific: Singapore, 2003.
3. Zhou CE, Liu GR, Lam KY. Three-dimensional penetration simulation using smoothed particle hydrodynamics. *International Journal of Computational Methods* 2008; **4**(1):671–691.
4. Liu MB, Liu GR, Zong Z. An overview on smoothed particle hydrodynamics. *International Journal of Computational Methods* 2008; **5**(1):135–188.
5. Nayroles B, Touzot G, Villon P. Generalizing the finite element method: diffuse approximation and diffuse elements. *Computational Mechanics* 1992; **10**:307–318.

6. Belytschko Y, Lu YY, Gu L. Element-free Galerkin methods. *International Journal for Numerical Methods in Engineering* 1994; **37**:229–256.
7. Liu WK, Jun S, Zhang YF. Reproducing kernel particle methods. *International Journal for Numerical Methods in Engineering* 1995; **20**:1081–1106.
8. Atluri SN, Zhu T. A new meshless local Petrov–Galerkin (MLPG) approach in computational mechanics. *Computational Mechanics* 1998; **22**:117–127.
9. Liu GR, Gu YT. A point interpolation method for two-dimensional solids. *International Journal for Numerical Methods in Engineering* 2001; **50**:937–951.
10. Wang JG, Liu GR. A point interpolation meshless method based on radial basis functions. *International Journal for Numerical Methods in Engineering* 2002; **54**:1623–1648.
11. Gu L. Moving kriging interpolation and element-free Galerkin method. *International Journal for Numerical Methods in Engineering* 2003; **56**:1–11.
12. Dai KY, Liu GR, Lim KM, Gu YT. Comparison between the radial point interpolation and the kriging based interpolation using in meshfree methods. *Computational Mechanics* 2003; **32**:60–70.
13. Tongsuk P, Kanok-Nukulchai W. Further investigation of element-free Galerkin method using moving kriging interpolation. *International Journal of Computational Methods* 2004; **1**:345–365.
14. Liu GR. *Meshfree Methods: Moving beyond the Finite Element Method*. CRC Press: Boca Raton, U.S.A., 2002.
15. Liu GR, Gu YT. *An Introduction to Meshfree Methods and their Programming*. Springer: Dordrecht, The Netherlands, 2005.
16. Liu GR, Zhang GY, Dai KY, Wang YY, Zhong ZH, Li GY, Han X. A linearly conforming point interpolation method (LC-PIM) for 2D solid mechanics problems. *International Journal of Computational Methods* 2005; **2**(4):645–665.
17. Zhang GY, Liu GR, Wang YY, Huang HT, Zhong ZH, Li GY, Han X. A linearly conforming point interpolation method (LC-PIM) for three-dimensional elasticity problems. *International Journal for Numerical Methods in Engineering* 2007; **72**:1524–1543.
18. Chen JS, Wu CT, Yoon S, You Y. A stabilized conforming nodal integration for Galerkin mesh-free methods. *International Journal for Numerical Methods in Engineering* 2001; **50**:435–466.
19. Li Y, Liu GR, Luan MT, Dai KY, Zhong ZH, Li G, Han X. Contact analysis for solids based on linearly conforming radial point interpolation method. *Computational Mechanics* 2007; **39**:859–877.
20. Liu GR, Li Y, Dai KY, Luan MY, Xue W. A linearly conforming RPIM for 2D solid mechanics. *International Journal of Computational Methods* 2006; **3**(4):401–428.
21. Liu GR, Zhang GY. Upper bound solution to elasticity problems: a unique property of the linearly conforming point interpolation method (LC-PIM). *International Journal for Numerical Methods in Engineering* 2008; **74**:1128–1161.
22. Zhang GY, Liu GR, Nguyen TT, Song CX, Han X, Hong ZH, Li GY. The upper bound property for solid mechanics of the linearly conforming radial point interpolation method (LC-RPIM). *International Journal of Computational Methods* 2007; **4**(3):521–541.
23. Zienkiewicz OC, Taylor RL. *The Finite Element Method* (5th edn). Butterworth Heinemann: Oxford, U.K., 2000.
24. Hughes TJR. *The Finite Element Method: Linear Static and Dynamic Finite Element Analysis*. Prentice-Hall: Englewood Cliffs, NJ, 1987.
25. Liu GR, Quek SS. *The Finite Element Method: A Practical Course*. Butterworth Heinemann: Oxford, 2003.
26. Zhang GY, Liu GR, Li Y. An efficient adaptive analysis procedure for certified solutions with exact bounds of strain energy for elasticity problems. *Finite Elements in Analysis and Design* 2008; DOI: 10.1016/j.finel.2008.06.010.
27. Wu HC. *Variational Principle in Elasticity and Applications*. Scientific Press: Beijing, 1982.
28. Pian THH, Wu CC. *Hybrid and Incompatible Finite Element Methods*. CRC Press: Boca Raton, FL, 2006.
29. Rong TY, Lee AQ. Generalized mixed variational principles and solutions of ill-conditioned problem in computational mechanics. Part 1: volumetric locking. *Computer Methods in Applied Mechanics and Engineering* 2001; **191**:407–412.
30. Liu GR. A generalized gradient smoothing technique and the smoothed bilinear form for Galerkin formulation of a wide class of computational methods. *International Journal of Computational Methods* 2008; **5**(2):199–236.
31. Li RH, Chen ZY. *Generalized Difference Methods for Differential Equations*. Jilin University Press: Changchun, China, 1994.
32. Timoshenko SP, Goodier JN. *Theory of Elasticity* (3rd edn). McGraw-Hill: New York, 1970.